Interconnected micro-mesoporous carbon nanofiber derived from lemongrass for high symmetric supercapacitor performance

by Rika Taslim

Submission date: 13-Apr-2023 02:31PM (UTC+0700)
Submission ID: 2063300078
File name: 15._JMRT_Juli_2022_Daun_serai.pdf (2.7M)
Word count: 8383
Character count: 44390

JOURNAL OF MATERIALS RESEARCH AND TECHNOLOGY 2022;19:4721–4732

Available online at www.sciencedirect.com

jmr&t Journal of Materials Research and Technology

journal homepage: www.elsevier.com/locate/jmrt

Original Article

Interconnected micro-mesoporous carbon nanofiber derived from lemongrass for high symmetric supercapacitor performance

Erman Taer [a,*], *Novi Yanti Effendi* [a], *Rika Taslim* [b,**], *Apriwandi Apriwandi* [a]

[a] Department of Physics, Faculty of Mathematic and Natural Sciences, University of Riau, Indonesia
[b] Department of Industrial Engineering, State Islamic University of Sultan Syarif Kasim Riau, Indonesia

ARTICLE INFO

Article history:
Received 22 December 2021
Accepted 30 June 2022
Available online 8 July 2022

Keywords:
Hierarchical porous
Nanofiber
High surface area
Porous carbon electrode
Supercapacitors

ABSTRACT

The hierarchical porous activated carbon nanofiber has been prepared and characterized from the biomass based of lemongrass leave waste (LG). The preparation process used a simple technique through impregnation of $ZnCl_2$ with low concentrations (0.5, 0.7 and 0.9) mol/L. These three concentrations were chosen to maximize the potential of LG to produce carbon nanoporous structures with high surface area. The preparation of activated carbon is performed by a one-step technique, including carbonization and physical activation at a temperature of 800 °C in N_2/CO_2 atmosphere. The three sample variations resulted in a very good amorphous structure according to the XRD pattern. The sample LG-0.7 has been known to have the best physical and electrochemical properties with an SSA reaching 1694 $m^2\ g^{-1}$ with a carbon content of 90.38%. Uniquely, the LG-0.7 sample has a combined morphological appearance of hierarchical pores such as sponges and nanofiber pores. This combined pore strongly supports the electrochemical properties of the carbon electrode with 256 F g^{-1}, a specific energy of 35.6 Wh kg^{-1} and a power density of 128.3 W kg^{-1} obtained using the GCD method. Electrochemical testing was carried out at a low potential of 0–1 V with a scan rate of 1 mV s^{-1} under the influence of an aqueous electrolyte of 1 M H_2SO_4. These results demonstrate the tremendous potential of lemongrass leaf waste as a raw material for the produce of porous carbon electrodes for high-performance supercapacitors.

1. Introduction

Ultra-electrochemical capacitors as great electrical energy storage devices have 10^6 times higher storage capacity than conventional capacitors, followed by excellent adsorption/desorption, almost infinite cycle stability, and excellent power density [1]. Furthermore, their eco-friendly, economical and efficient main components make them the best choice in the development of optimum energy conversion and storage

* Corresponding author.
** Corresponding author.
E-mail addresses: erman.taer@lecturer.unri.ac.id (E. Taer), rikataslim@gmail.com (R. Taslim).
https://doi.org/10.1016/j.jmrt.2022.06.167

systems [2]. According to the energy storage mechanism, supercapacitors are divided into electric double-layer capacitors (EDLC) and pseudo-capacitors [3]. The EDLC mechanism is based on the electrostatic adsorption/desorption of ions from the electrolyte on the surface of the electrode which is influenced by Coulomb forces to form an electric double layer on the surface of the basic components [4]. Meanwhile, pseudo-capacitors are based on redox reactions of heteroatoms on fast electro-active surfaces [3,5]. However, their energy density is relatively low compared to batteries and fuel cells. Therefore, it is necessary to develop the next generation of supercapacitor devices with high energy density without losing other advantages.

The main components of activated carbon (AC) based electrodes are considered as key candidates in writing the latest generation of electrochemical ultra-capacitors due to their abundant source availability, cost-effectiveness, high surface area, and superior electrochemical stability [6,7]. What's even more surprising is that their energy density can compete with other generations of batteries, even with fuel cells. In recent decades, activated carbon can be obtained from waste biomass sources which are very abundantly available, making them the first candidates in the development of a new generation of supercapacitors. In addition, biomass-based activated carbon is claimed to have a relatively environmentally friendly, simple preparation process, does not require complex instruments, cost-effective and time-saving. Among the potential biomass as a source of activated carbon for supercapacitor applications are pitaya peel [8], coffee grounds [9], bark [10], wood [11], bamboo [12], palm oil [13], tofu dregs [14], etc. However, activated carbons generally have relatively lower capacitive properties with limited charge flow rates and poor conductivity. The development and modification of their structure are continuously being performed in order to meet these challenges. Recent studies have shown that these shortcomings can be overcome by designing 3D connected micro-mesopore pore structures followed by 2D nanostructures in particular nanofibers. The micropore structure contributes to providing a high surface area to absorb more ions thereby enabling the formation of a rich-electrically layer. The mesoporous structure functions as a nearly barrier-free ion channel to initiate rapid ion flow at the electrode surface. The combination of the two connected hierarchically allows the device to produce high capacitive properties with the best stability. As reported by Xu et al. (2021), electrochemical properties were drastically improved through hierarchical porous carbon via a novel strategy using melamine matched with potassium hydroxide [15]. Compared to others, these activated carbons are capable of producing a very high surface area of 3344 $m^2\ g^{-1}$ with their capacitive properties reaching 520 F g^{-1}. Activated carbon-based on mesophase pitch and biomass sawdust have succeeded in obtaining a hierarchical pore structure from the combination of micro-meso-, and macropores to improve the capacitive properties of symmetric supercapacitors [16]. Furthermore, they markedly demonstrated the potential for self-doped heteroatoms to confirm additional pseudo-capacitance effects. However, they failed to show an increase in the conductivity of the raw material. Meanwhile, 2D nanostructures, especially abundant nanofibers, significantly increase the high conductivity of the electrode material [17,18]. Interestingly, cellulose is the main source of nanofibers in biomass-based porous activated carbon, whereas some biomasses are high in cellulose content. This is very advantageous for the electrode material. Several previous studies reviewed the potential of biomass as a carbon nanofiber source to enhance high-performance supercapacitors such as pineapple leaves [19], coconut shells [20], mission grass [21], etc. Therefore, the combination of the 3D hierarchical pore structure with the 2D nanofiber structure is very advantageous in enhancing the electrochemical properties of supercapacitors. However, it is very difficult to find the potential of organic waste as a porous carbon source that has a combination of these material properties.

Through intense study, we believe lemongrass leaves have great potential in providing a 3D hierarchical pore structure with rich nanofibers as a source of activated carbon. Lemongrass (*Cymbopogon Citratus*) is a type of grass plant with a long leaf structure like that of thatch which is well-known in Asia as a spice ingredient because it has a distinctive aroma and taste. Lemongrass productivity in 1 ha can produce 1000 clumps with wet leaves of at least 0.5 kg per clump. In processing, lemongrass stalks are separated from the leaves as a kitchen spice and traditional medicine. Meanwhile, lemongrass leaves are used as animal feed, organic fertilizer and the rest becomes waste. The high production of lemongrass in several areas indicates the increasing number of lemongrass leaves which have the potential to become waste because the processing is not yet optimal. Moreover, almost lemongrass leaves consist of cellulose which has great potential as an active carbon base material [22]. These two reasons are used as the basis for choosing lemongrass leaf waste as the basic material for making porous activated carbon electrodes.

Based on the above considerations, we report a facile approach to obtain 3D hierarchical porous activated carbon with abundant nanofibers as electrode base material to improve the symmetric electrochemical properties of supercapacitors. Lemongrass leaves as a carbon source were chemically impregnated in zinc chloride solution varied including 0.5 mol/L, 0.7 mol/L, and 0.9 mol/L at high-temperature pyrolysis. To add to their advantages, the porous activated carbon is prepared in the form of a coin without the addition of a binder. The obtained porous activated carbon has significantly demonstrated a 3D hierarchical pore structure followed by abundant nanofibers. The resulting specific surface area is 1694 $m^2\ g^{-1}$ Through a two-electrode system, the best electrode obtained high capacitive properties of 201 F g^{-1} in 1 M H_2SO_4 electrolyte. Moreover, their energy density has shown a potential of 17.89 Wh kg^{-1} at a current density of 1 A g^{-1}. These results demonstrate the great potential of lemongrass leaves waste as a source of 3D hierarchical porous activated carbon with rich nanofibers to enhance the electrochemical properties of supercapacitor energy storage devices.

2. Materials and methods

2.1. Materials

The basic material for preparation activated carbon based on lemongrass (LG) leaves biomass (*Cymbopogon Citratus*) were

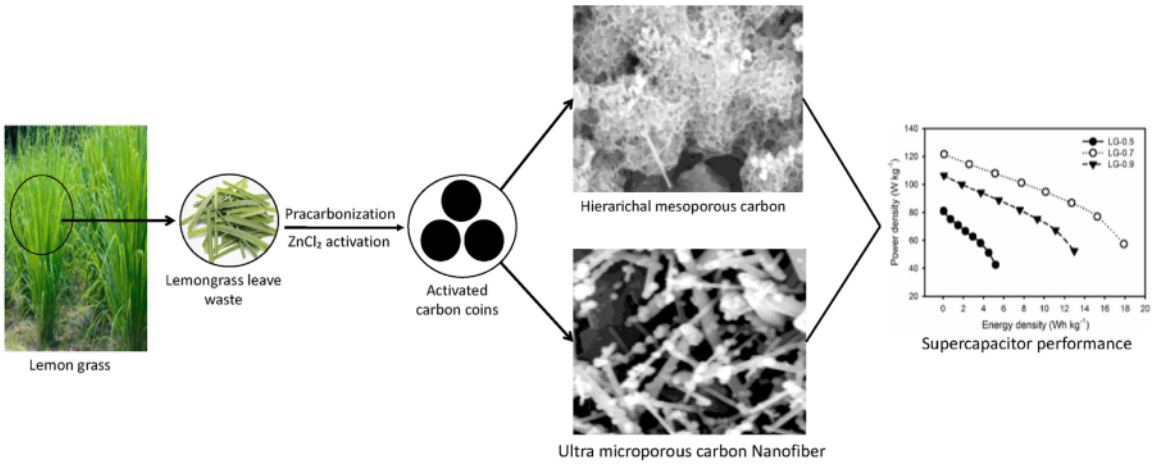

Scheme 1 – Preparation of hierarchical porous carbon nanofiber based on lemongrass leaf waste.

collected from agricultural waste in Pekanbaru, Riau, Indonesia. The LG is separated from the stem, then cut into small pieces of 3–5 cm. LG samples were dried using sunlight and a 110 °C drying oven for 3 days. Pre-carbonization of LG samples to 250 °C for 2.5 h using a vacuum oven to brittle and improve self-adhesive properties. Followed by refining the particle size of the carbon sample using a mortar and ball milling tool for 20 h. The LG sample powder was sieved to obtain a uniform carbon particle size <60 m. Chemical activation was carried out using $ZnCl_2$ activation agent with different concentrations. The activation agent was purchased from Merck KgaA, Germany. Aquades and pH meters were used for the preparation and neutralization of monolith samples.

2.2. *Preparation of hierarchical porous carbon nanofiber*

Activated carbon LGs were prepared using a single-stage integrated chemical activation and combustion method under the influence of N_2 and CO_2 gases. The chemical activator $ZnCl_2$ was chosen as the dependent variable, with different concentrations of activator 0.5 M, 0.7 M and 0.9 M as independent variables in the prepared of activated carbon LGs. The mass ratio of $ZnCl_2$ to LGs was 1:3, 1.5:3, and 2:3 for LG-0.5, LG-0.7, and LG-0.9, respectively. Each variation of $ZnCl_2$ concentration was homogenized with 150 ml of distilled water and 30 g of carbon. This was followed by printing the LGs carbon powder into a monolithic coin shape with a solid and not brittle texture using a hydraulic press. LGs carbon coins are pyrolyzed using a single-stage integrated method with carbonization to a temperature of 600 °C of N_2 gas and physical activation to a temperature of 800 °C of CO_2 gas. Carbonization aims to evaporate elements other than carbon such as volatile compounds thus purer carbon is produced. Physical activation aims to increase pore size and open new pore structures. Then the carbon coins are neutralized by washing them with distilled water. In detail, the process of making LGs activated carbon with a combined pore appearance of

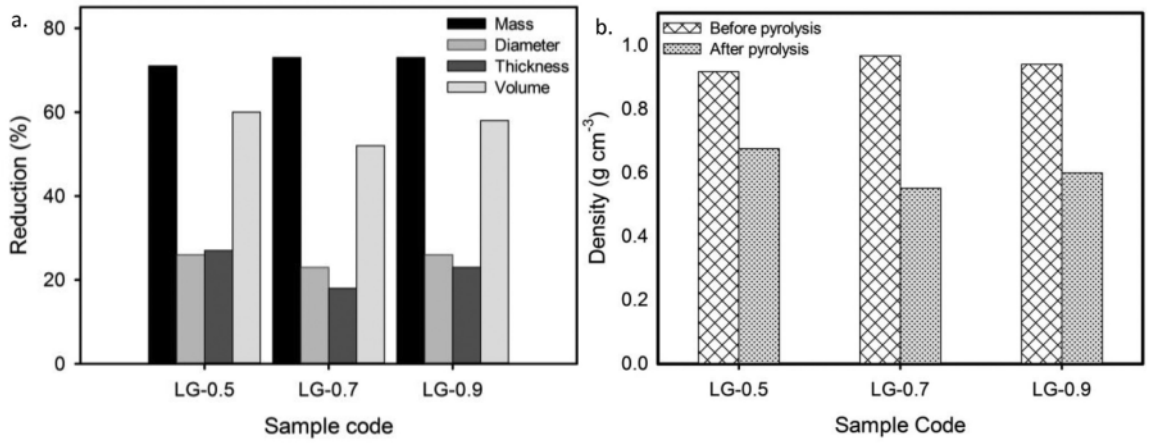

Fig. 1 – (a) Depreciation of mass, diameter, thickness and volume (b) Decreased density carbon nanofiber lemongrass-based.

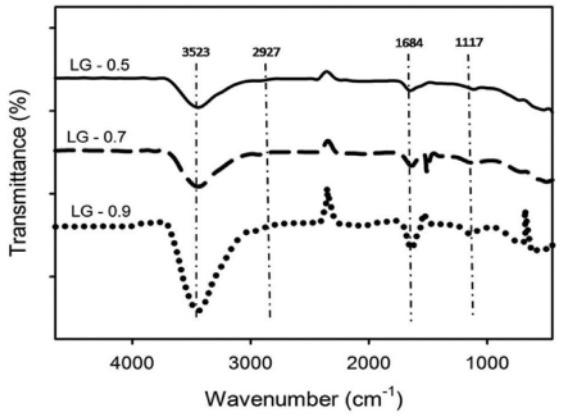

Fig. 2 – FTIR spectrum of lemongrass activated carbon.

hierarchal mesoporous and Ultra microporous carbon Nanofiber with a surface area of up to 1694 $m^2\ g^{-1}$ is shown in Scheme 1.

2.3. Material characterization

The decrease in density is the basic characterization of determining the physical properties of activated carbon monolith LGs based on the decrease in mass, diameter and thickness after the pyrolysis process. Fourier Transform Infra Red (FTIR) was carried out to determine the compound content, level of wettability and absorption through functional groups. FTIR uses an infrared light source that is converted into waves and then forwarded to carbon powder samples using a Shimadzu Prestige 21 Nicolet Avatar 360 IR tool. The light beam is captured by a detector connected to a monitor to display the FTIR spectrum in the range of 450–4500 cm^{-1} wavenumber. The characterization of the uptake and release of N_2 gas was carried out using the Brunauer Emmett Teller (BET) and Barrett Joyner Halanda (BJH) methods. BET and BJH

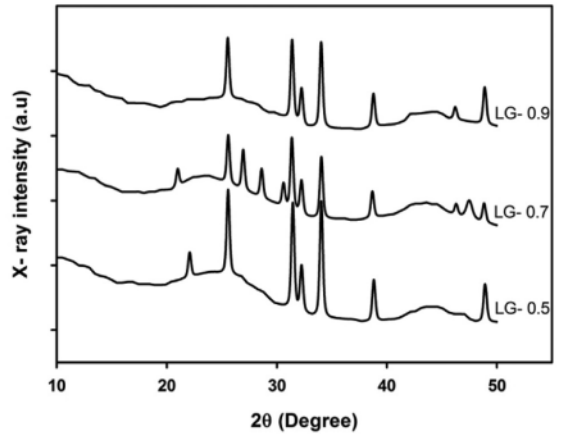

Fig. 3 – XRD pattern for LG-0.5, LG-0.7 and LG-0.9.

were used for the calculation of the sample surface area (S_{BET}) and the pore size distribution (PSD) based on the amount of N_2 gas absorbed. The test was carried out at 55 points with a degassing temperature of 300 °C for 3 h at a relative pressure of ~0.95. Scanning electron microscopy (SEM) was used to observe the morphological pore structure in the fracture cross-section of the carbon pellets. SEM results in the form of dark and light images with a magnification of 20,000 × and 40,000 × . Energy dispersive X-ray (EDS) is performed to inform the percentage of elemental content in the sample. This characterization uses the Phenom Pro G6 Desktop SEM tool which is a versatile, durable, robust and easy application with high brightness using a Cu electron source designed to expand the capabilities of the research facility. X-ray diffraction was used to determine the degree of crystallinity of samples with a Cu-Kα ray source of 1.5418 Å in the 2θ (15°–55°) scale range. This measurement uses the Philip X-Pert Pro PW3060/10 Pananalytical Brand tool.

2.4. Confirmation of electrochemical properties

Cyclic voltammetry (CV) and Galvanostatic charge-discharge (GCD) methods were used to determine the electrochemical properties of LGs waste supercapacitor cells. The test used a membrane separator from duck eggshells in 1 M H_2SO_4 aqueous electrolyte. Two similar electrodes were arranged like a sandwich layer for CV and GCD characterization. Characterization using the Physics CV UR Rad-Er 5841 tool which is controlled with Cyclic Voltammetry CV V6 Software and CD UR Rad-Er 2018 with the VersaStat II Princeton Applied Research calibration instrument with an error percentage of ±6.0%. LGs electrode under the influence of 1 M H_2SO_4 electrolyte as a source of ionic charge at a low potential of 0–1000 mV. The CV method used a scan rate variation of 1, 2, 5 and 10 mV s^{-1}, for GCD a low scan rate of 2 mV s^{-1} was used. The CV characterization output is in the form of a distorted rectangular curve display with a specific capacitance value based on the area of the curve. The output of the GCD method in the form of a distorted triangle with a long discharging time can increase the performance of the supercapacitor cell. The energy density and power density was calculate by Eqs (1) and (2) [23,24].

$$E_{sp} = \int IV\,dt \tag{1}$$

$$P_{sp} = \frac{E_{sp}}{t} \tag{2}$$

where Δt is discharge time (s), ΔV is discharge voltage (V), I is current (A), E_{sp} is energy density (Wh kg^{-1}), and P_{sp} is power density (W kg^{-1}).

Table 1 – Chemical contents of LGs samples.

Sample codes	Elemental status (atomic weight (%))				
	C	O	Si	Ca	Zn
LG-0.5	93.13	5.99	0.23	0.22	0.42
LG-0.7	93.20	6.25	0.26	0.3	0.00
LG-0.9	92.81	6.75	0.32	0.23	0.31

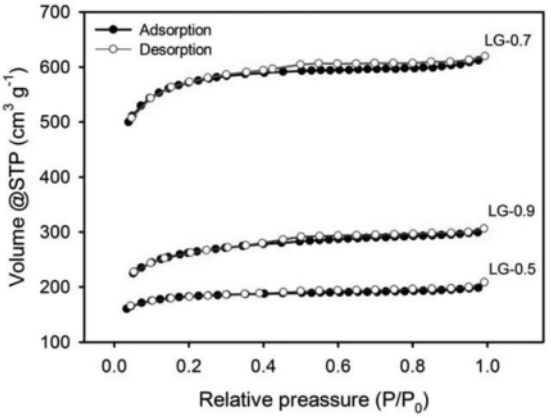

Fig. 4 – N_2 gas absorption. desorption curve for samples LG-0.5, LG-0.7 and LG-0.9.

3. Results and discussions

3.1. *Materials properties analysis*

Density is an initial confirmation to evaluate the material properties of the carbon nanofiber lemongrass-based binder-free material. Density was analyzed based on the decrease in mass, diameter and thickness in before and after high-temperature pyrolysis which was influenced by the decomposition of volatile compounds other than carbon such as cellulose, hemicellulose, and lignin [25,26]. Fig. 1a illustrated the shrinkage of mass, diameter, thickness and volume of LGs carbon nanofiber binder-free. As shown in Fig. 1b, LG-0.5, LG-0.7 and LG-0.9 had initial densities 0.916, 0.966 and 0.939 g cm^{-3} which decreased to 0.675, 0.55 and 0.599 g cm^{-3} after the pyrolysis process. The addition of $ZnCl_2$ concentration from 0.5 mol/L to 0.7 mol/L can maximize the evaporation of volatile compounds up to 43%. Therefore, the sample LG-0.7 is considered to have optimum porosity based on the amount of volatile elements. The addition of an activation agent up to 0.9 mol/L possessed higher density of 9% then LG-07 caused by excessive evaporation thus the sample undergoes pore collapse [27,28]. The decrease in density for this sample is in accordance with research that has been performed previously with shallot peel waste as the raw material [29].

The FTIR spectra of activated carbons LG-0.5, LG-0.7 and LG-0.9 were tested at a wavenumber of 450–4500 cm^{-1} as shown in Fig. 2. Based on the measurement results of the FTIR spectrum peaks, the samples of LGs experienced a slight shift which was influenced by chemical bonds between functional groups. It can be seen that the peak of the strain at wavenumber 3523 cm^{-1} comes from the hydroxyl functional group (O–H) [30]. The addition of $ZnCl_2$ activator concentration on activated carbon of lemongrass leaves can increase the hydroxyl transmittance. Pseudocapacitance properties arise from the presence of hydroxyl strain which can increase the wettability of porous carbon electrodes thus as to increase the performance of the supercapacitor. However, the presence of hydroxyl groups that exceed the optimum conditions can damage the pore structure of the carbon, thereby reducing the capacitance. As happened in the sample LG-0.7 has a transmittance of 11% while LG-0.9 has 20% which is influenced by the addition of concentration. This causes the specific capacitance value of LG-0.7 to be greater than LG-0.9 based on the magnitude of the decrease in density of LG-0.7. At the wave number 2927 cm^{-1} there is a stretch of aliphatic functional group (C–H) which includes volatile hydrocarbon compounds. Wavenumber 1684 cm^{-1} indicates volatile hydrocarbon compounds (C=C) in the lemongrass leaf carbon samples which support carbon purity. At the wave number 1117 cm^{-1} there is a C–O–C functional group [31]. Furthermore, based on the graph of the FTIR measurement results for wave numbers below 600 cm^{-1}, the hydroxyl (OH) functional group of water decreased exponentially. The 0.7 M $ZnCl_2$ in sample LG-0.7 has optimum hydroxyl and carbonyl functional groups so that a sample with high carbon purity and absorption capacity is produced for the manufacture of supercapacitors from lemongrass leaf biomass.

The LGs samples were evaluated for their degree of crystallinity for each variation in $ZnCl_2$ concentration OF LG-0.5, LG-0.7 and LG-0.9 using X-ray diffraction patterns, as shown in Fig. 3. XRD pattern possess two broad peaks for all sample variations in the d_{100} and d_{002} planes with diffraction angles of 22°–25° and 42°–45° which indicate the presence of a hexagonal structure [32]. This broad peak is indicated by its amorphous nature with an irregular arrangement of carbon biomass-based [33]. The amorphous properties were found in the sample LG-0.7 which resulted from the abundance of micropores [34]. In addition, there are very few sharp peaks at certain diffraction angles. These results are consistent with studies using different biomasses such as banana leaves [35], *moringa oleifera* stem [36], peanut shells [37]. This sharp peak informs the presence of elements other than carbon that are crystalline in the sample according to the EDS test results such as oxygen, silica, calcium, zinc and chlorine. According to (JCPDS No. 89–1668) sharp peaks at angles of 29°–45° for all samples are indicated by elemental SiO_2 [24]. Elemental oxygen is read at a diffraction angle of 32°–35° and according to (JCPDS No. 82–1690) at a diffraction angle of 39° indicated by elemental $CaCO_3$ [38].

The element contents of activated carbon was confirmed by EDS analysis. Table 1 display the percentage of element status for LG-0.5, LG-0.7 and LG-0.9. They have a high carbon content of 92.81–93.20%. The addition of activator concentration from 0.5 M to 0.7 M can increase the percentage of carbon gradually from 93.13% to 93.20%. This is due to high carbon etching and effective decomposition of non-carbon compounds, including organic acids, volatiles, and tars perfectly. Oxygen in the sample also increased from 5.99% to 6.25%. The high carbon content in the sample LG-0.7 is indicated by the optimization of the activator concentration that supports the release of elements other than carbon during the pyrolysis process. Elements of oxygen, silica, calcium, zinc and chlorine are natural constituents of biomass that are still remaining during the combustion process in small amounts [39]. The remaining oxygen element acts as self-doping which can produce pseudocapacitance which helps increase the

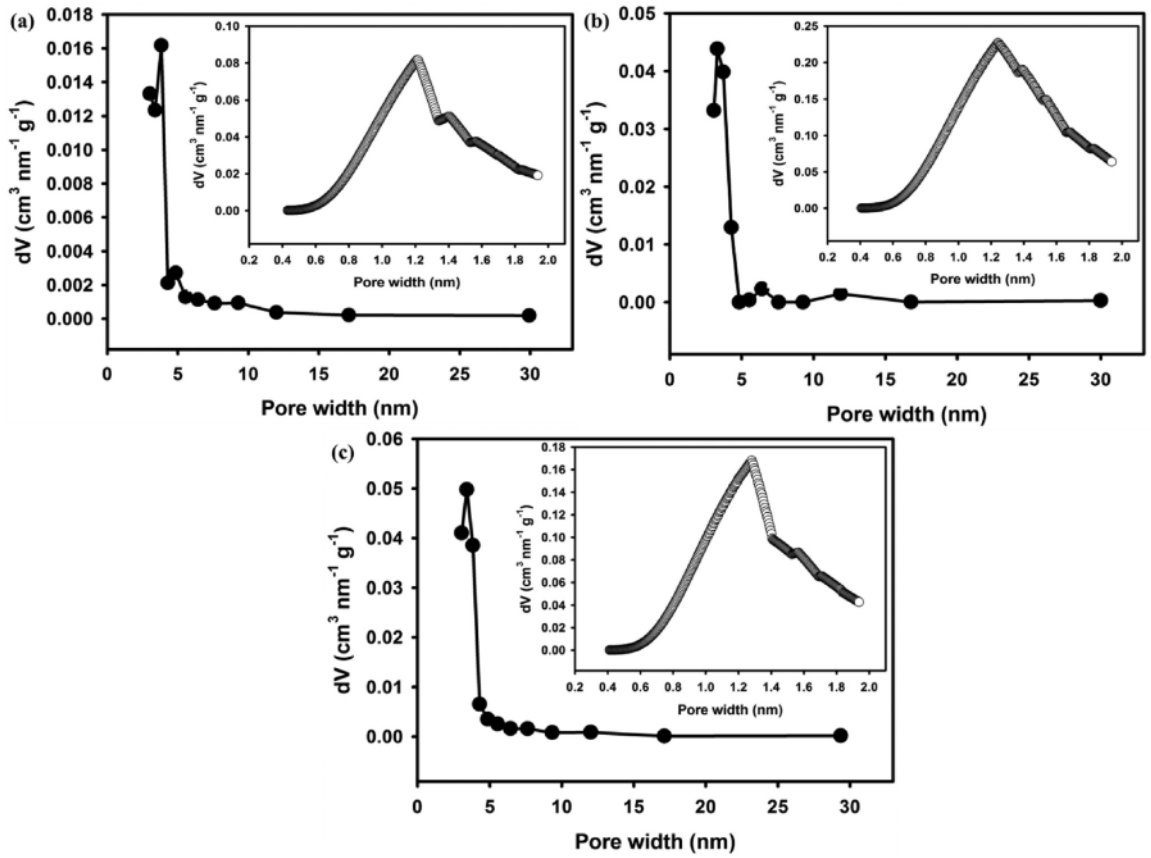

Fig. 5 – Pore size distribution of LG-0.5, LG-0.7 and LG-0.9.

capacitance value [40]. However, the addition of the activator concentration to 0.9 M in lemongrass leaves carbon can reduce the percentage of carbon and oxygen content again. This is because the addition of $ZnCl_2$ activator concentration exceeding the optimum condition can evaporate the carbon element during the pyrolysis process, so that the percentage of carbon in the sample LG-0.9 is reduced. This EDS result is in accordance with previous research using wheat husk and soybean biomass with carbon percentages of 87.96% and 86.19% [41,42].

The porosity properties of activated carbon LGs was analyzed by two methods of Brunauer Emmett Teller (BET) and Barrett Joyner Halanda (BJH). BET to obtain the surface area according to the N_2 absorbtion/desorption (see Fig. 4.) and BJH to determine the pore size distribution (see Fig. 5). The characterization results for LGs show an type I/IV isotherm curve with H4 type hysteresis loops. At P/P0<0.2 showed an increase in the absorption volume due to the dominant microporous effect, especially in the sample LG-0.7 with a micropore surface area of almost 90%. When the pressure is increased by $0.4 < P/P_0 < 0.91$ followed by H4 hysteresis loop indicated the presence of abundant mesopores. The addition of further pressure $P/P_0 > 0.92$ informed the availability of macropores in activated carbon LG-5. Furthermore, Table 2 summerize the surface area, pore volume and average pore diameter of LGs.

The difference in concentration of $ZnCl_2$ activator on activated carbon LGs gives a high effect on the specific surface

Table 2 – Specific surface area, volume and pore width of LGs samples.

Sample Code	S_{BET} ($m^2\ g^{-1}$)	S_{micro} ($m^2\ g^{-1}$)	S_{meso} ($m^2\ g^{-1}$)	V_{tot} ($cm^3\ g^{-1}$)	V_{micro} ($cm^3\ g^{-1}$)	V_{meso} ($cm^3\ g^{-1}$)	D_{aver} (nm)
LG-0.5	536	480	56	0.322	0.253	0.069	2.402
LG-0.7	1694	1538	156	0.958	0.802	0.156	2.262
LG-0.9	795	661	134	0.473	0.341	0.132	2.378

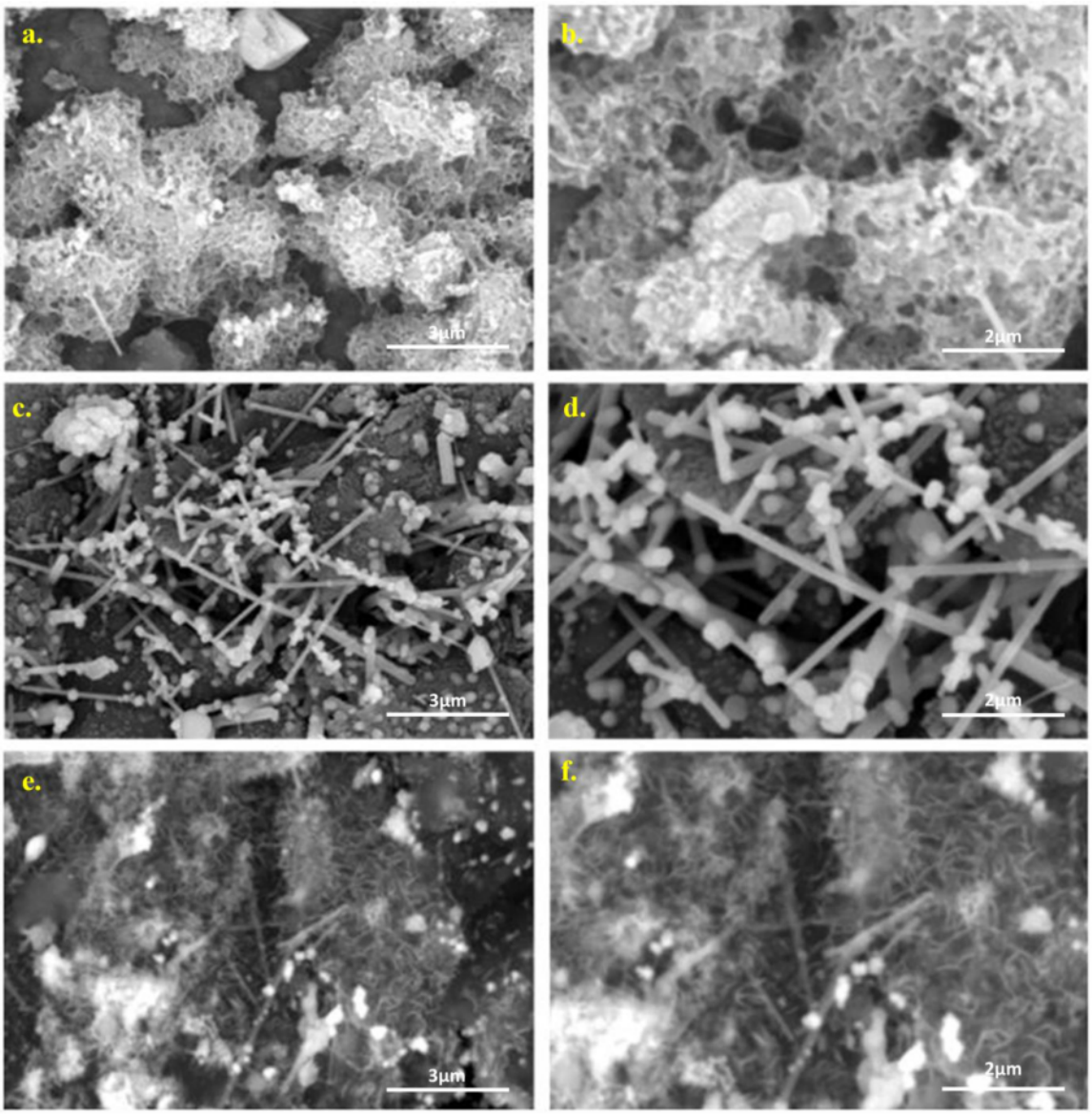

Fig. 6 – Surface morphology of activated carbon nanofiber lemongrass-based.

area (SSA) and pore volume. The addition of 0.5 M $ZnCl_2$ activator concentration to 0.7 M increased SSA and pore volume up to 3 times. This is because as a reducing agent, $ZnCl_2$ can break the lateral bonds in the cellulose molecule to produce activated carbon with a high surface area [43]. The distribution of the dominant micropores in the activated carbon sample of lemongrass leaves reached 90% with an average pore diameter of 1.3 nm can be seen in Fig. 6. The dominant micropores can provide a high surface area that supports electrochemical performance through maximum ion absorption with high energy density [44]. The addition of the activator concentration also develops micropores into mesopores and the formation of new micropores that support the optimization of SSA. The sample LG-0.7 produces a surface area of up to 1694.96 m^2g^{-1} which is supported by EDS analysis with a carbon content of up to 90%. In addition, the optimization of SSA LG-0.7 is strengthened by the appearance of hierarchical pores of porous and fiber in nanometer scale. The addition of $ZnCl_2$ concentration that exceeds the optimum conditions up to 0.9 mol/L can induce pore coalescence which causes a decrease in the return of SSA and pore volume due to pore collapse [27]. LGs activated carbon with a high surface

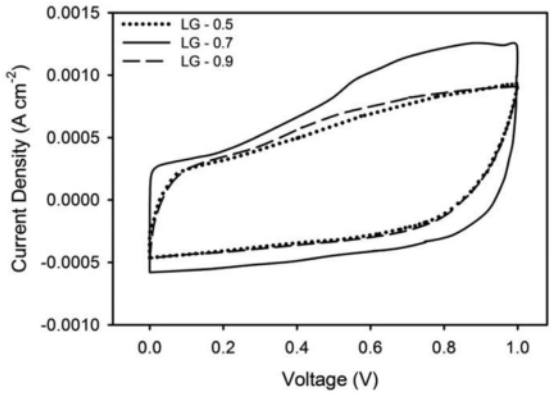

Fig. 7 – CV curves for LG-0.5, LG-0.7 and LG-0.9.

area is produced through a simple process and without the addition of adhesives. The surface area of activated carbon of lemongrass leaves with $ZnCl_2$ activator 0.7 mol/L can compare with other studies using cotton stalk biomass 1227 m^2g^{-1} [45], kraft lignin 2424.8 m^2g^{-1} [46], chitosan 3646 m^2g^{-1} [47]. However, the technique used to produce a high surface area in other studies has several weaknesses such as using a corrosive gel electrolyte, using N and P doping, using additional Polyvinylidene Fluoride (PVDF) adhesives and the use of argon which is relatively expensive. During the carbonization process.

The morphological structure of porous carbon lemongrass leaves-based was examined in depth through scanning electron microscopy (SEM) at different magnifications (20,000× for Fig. 6. (a) (c) and (e) and 40,000X for Figure (b), (d), and (f)). Chemically impregnated precursors of biomass at high temperatures can significantly decompose their biological components and chemical compounds and it is indicated to influence the morphological structure of the obtained porous carbon, as discussed extensively previously [48,49]. Based on the consideration of porosity, amorphousness, and wettability properties, lemongrass leaves precursors impregnated with $ZnCl_2$ in a solution of 0.7 mol/L at high-temperature pyrolysis were evaluated for their morphological structure as shown in Fig. 6. In fact, the porous carbon LG-0.7 exhibits great morphological structures potential. The superior morphology includes 3D connected hierarchical pores and dense nanofiber structures to support the high performance of the electrode material as an electrochemical energy storage device [21,50]. Fig. 6a plays the hierarchical pore sponge-like morphology structure which varies across enrich-mesopores around 5–20 nm. In addition, at a higher zoom area (see Fig. 6b), the LG-0.7 sample confirmed high macroporosity in the nano to micron scale. High-temperature pyrolysis allows complete evaporation of biological components and optimum development of the carbon framework resulting in a combined meso-macropore structure on the LG-0.7 surface. The combination of these two pores which are connected hierarchically allows activated carbon to have an "expressway" ion transport pathway and allows them to move in all directions in 3D space resulting in high power density and low internal resistance [51]. Furthermore, the SEM micrographs in Figs. 7c and 6d display clearly confirmed 2D nanofiber structures. $ZnCl_2$ impregnation allows the decomposition of complex compounds of hemicellulose, cellulose, and lignin in which hemicellulose and lignin attached to the cellulose decompose optimally [52,53]. Cellulose as a source of fibers as well as a biomass precursor is optimized through salt degradation to produce a nanofiber structure. The abundant nanofiber structure on a diameter scale of about 4–119 nm allows controlled micropore growth thereby enabling the porous carbon to have abundant active sites for more ion diffusion. This certainly initiates the formation of a high electric double layer in supercapacitor electrochemical energy storage devices. Moreover, LG-0.7 surprisingly displayed a combination of hierarchical 3D interconnected pore morphology and dense nanofiber structure, as shown in Figs 6e and f. SEM micrographs in Fig. 6e and e confirm the hierarchical pore structure in the sub-mesoporous sclera around 2–5 nm. It also confirmed the enrich-nanofiber structure in the 6–15 nm range. The combination of these morphological structures significantly results in superior material structures that initiate the formation of highly active sites, unimpeded ion transport pathways, high conductivity, and low internal resistance. This was confirmed more thoroughly by analyzing the electrochemical properties of cyclic voltammetry and galvanostatic charge–discharge techniques.

3.2. *Electrochemical behavior analysis*

The contribution of microporosity, high surface area, and combination of 3D and nanofiber pore hierarchies to the electro-active properties of lemongrass-based carbon electrodes were evaluated in a complex manner through cyclic voltammetry (CV) and galvanostatic charge–discharge (GCD) techniques in 1 M H_2SO_4 electrolyte. Fig 7 demonstrates the electrochemical characteristics of a supercapacitor cell in a two-electrode system via a CV profile. LGs supercapacitor cells exhibit a quasi-square CV profile at a scan rate of 1.0 $mV\ s^{-1}$

Table 3 – Comparison of electrochemical properties of various sources of electrode materials.

Sources	Activation agent	SSA ($m^2\ g^{-1}$)	S_{micro} ($m^2\ g^{-1}$)	S_{meso} ($m^2\ g^{-1}$)	C_{sp} ($F\ g^{-1}$)	E_{sp} ($Wh\ kg^{-1}$)	P_{sp} ($W\ kg^{-1}$)	Ref
Cotton stalk	KOH	1227.2	–	–	111	12.5	900	[45]
Chitosan	H_3PO_4	3646	1253	2393	586	28.1	450	[47]
bacterial cellulose	KOH	1554	1311	243	430	–	–	[44]
Olive pomace	KOH	2481.8	1451.7	1000,1	–	–	–	[57]
Ammonia solution	KOH	3259	2478	781	225	31.25	112.6	[58]
Lemongrass	$ZnCl_2$	1695	1538.2	156.8	256	35.6	128.3	This study

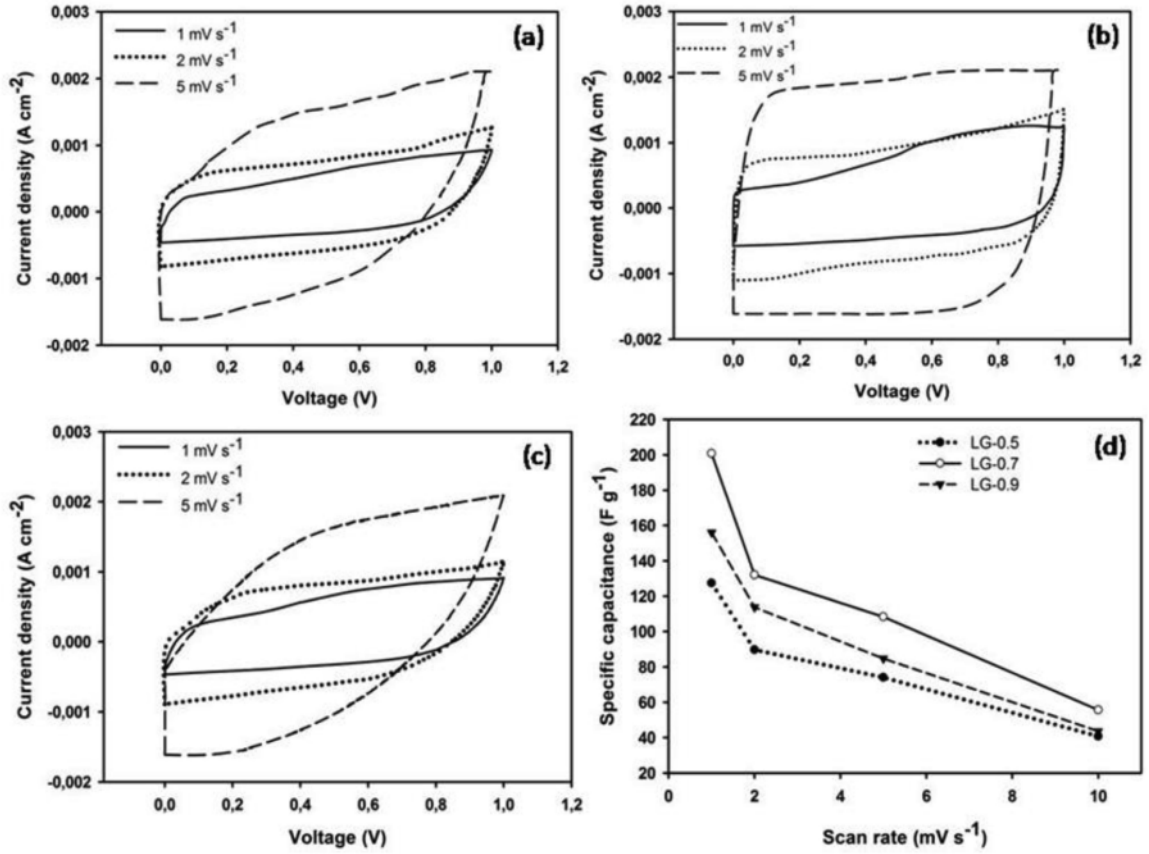

Fig. 8 – CV curve in different scanning rate of (a) LG-0.5, (b) LG-0.7, (c) LG-0.9 and (d) Specific capacitance vs. different scan rate.

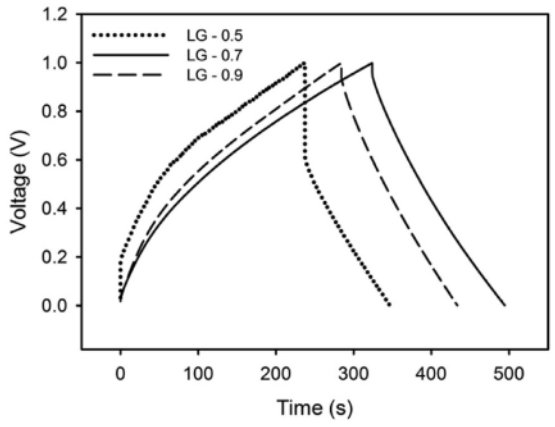

Fig. 9 – GCD profiles for samples LG-0.5, LG-0.7 and LG-0.9.

initiating ion transport forming a normal electrical double layer [54]. Furthermore, the pseudo-capacitive effect is seen quite clearly in LG-0.7 and LG-0.9 which is characterized by a current hump in the 0.4–0.6 V voltage window. In addition, the CV hysteresis profile confirmed their capacitive nature, where the strongest hysteresis was found at LG-0.7 with a specific capacitance of 201 F g^{-1}, followed by LG-0.9 and LG-0.5 of 156 and 127 F g^{-1}, respectively. Chemical activation at concentrations increasing from 0.5 mol/L to 0.7 mol/L significantly increased the symmetric capacitive properties of the supercapacitors by almost 1/3. This is because the contribution of their porosity has changed drastically from LG-0.5 to LG-0.7. The surface area of LG-0.7 is almost 3 times higher than that of LG-0.5, as shown in Table 2. As is generally known, the large specific surface area allows the carbon electrode to provide a highly active site for the ions to diffuse to form an electrical double layer. In addition, abundant oxygen heteroatoms, as shown in Table 1, add to the pseudo-capacitance effect on their electrochemical properties. The combination of these material properties can significantly increase the high capacitive properties of the LG-0.7 electrode. Meanwhile, the addition of a higher $ZnCl_2$ concentration up to 0.9 mol/L performed specific capacitance degradation to 156 F g^{-1}. This is indicated by their relatively degraded porosity, as shown in Table 3. The addition of a higher concentration of $ZnCl_2$ allows more grinding of the carbon

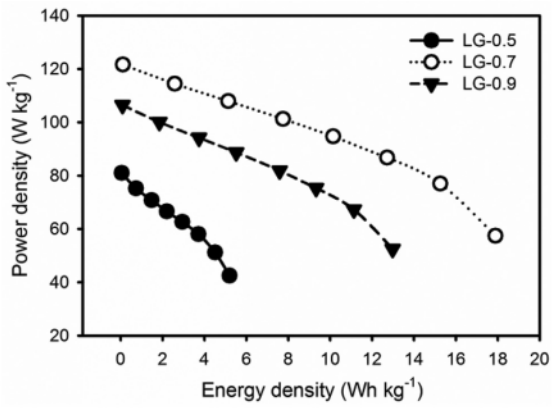

Fig. 10 – Ragone plot for samples LG-0.5, LG-0.7 and LG-0.9.

framework thus it can reduce its specific surface area. Although LG-0.9 has abundant mesoporosity nevertheless they cannot possess the highest capacitive properties at the LG-0.9 electrode. Fig. 9a–9c shows the CV profiles of the LGs electrodes at different scanning rates. In general, they still retain a quasi-square shape which results in normal electrical double layer properties. At higher scan rates, the LGs electrode did not display a pseudo-capacitance effect confirming the relatively weak self-heteroatom doping. Meanwhile, different scan rates have an impact on the capacitive properties of LGs, as shown in Fig. 9d. Scan rates higher from 1.0 to 10.0 mV s^{-1} simultaneously degrade the specific capacitance of LGs. Nonetheless, LG-0.9 can maintain a maximum specific capacitance of 68% due to the abundant mesoporosity contribution [55].

Evaluation of the electrochemical properties of LGs, especially specific capacitance, energy density, and power density were evaluated in depth through the galvanostatic charge–discharge (GCD) technique. Fig. 9 shows the GCD profile of the LGs electrode at a current density of 1.0 A g^{-1} in the 1 M H_2SO_4 electrolyte. The imperfect isosceles triangle shape in the GCD profile confirms the normal electrical double layer properties [56], as is also shown in the CV profile. Furthermore, different charge and discharge times indicate the occurrence of ion degradation due to self-heteroatom indicating the pseudo-capacitance of the LGs electrode. In addition, the length of charge–discharge time significantly confirms the capacitive nature of the sample. LG-0.5 has the smallest charge and discharge time indicating the lowest capacitive property of 174 F g^{-1}. In addition, the iR drop was found clearly on the LG-0.5 electrodes indicating their relatively large internal resistance of 0.4Ω. The addition of ZnCl2 concentration to LG-0.7 can significantly increase the specific capacitance up to 256 F g^{-1} with almost loweriR drop. These data trends are relatively consistent with CV analysis, although the values they get are slightly different. This is due to several reasons, including (i) the high surface area (see Table 3) due to the rich micropores enabling the LG-0.7 electrode t[46]ave abundant active sites for ions to diffuse to form a large electrical double layer at the electrode/electrolyte interface. (ii) The combination of hierarchical pores connected in 3D (see SEM micrograph) allows ions to move freely in all directions thus the number of currents increases drastically. (iii) The rich nanofiber structure allows the electrode to have high conductivity and it results in a very weak internal resistance. The combination of these three superior material properties significantly increases the specific capacitance, energy density, and power density of the LG-0.7 electrode (Fig. 10). Meanwhile, LG-0.9 shows a triangular shape with charge–discharge time between LG-0.5 and LG-0.7 confirming the reduced capacitive properties up to 208 F g^{-1}. This result is relatively the same as the CV analysis (see Fig. 8). Moreover, the energy density and power density of LGs were also evaluated as shown in Fig. 10. LG-0.7 with all its superior material properties exhibits a markedly high energy density of 23 Wh kg^{-1} with an optimum power density of 98.87 W kg^{-1} at a current density of 1.0 A g^{-1} in 1 M H_2SO_4 electrolyte. It was followed by LG-0.9 and LG-0.5 at 17 and 11 Wh kg^{-1} respectively at their power densities of 88 and 76 W kg^{-1}. These results were also compared with other carbon sources, as shown in Table 3.

4. Conclusion

Finally, it has been confirmed that the hierarchical porous and naofiber are unique structures of the activated carbon pores of 0.7 mol/L $ZnCl_2$ impregnated lemongrass leaves. It is produced from a simple technique, without the addition of adhesives and is cost effective. LG activated carbon treatment based on different concentrations of $ZnCl_2$ activator (0.5, 0.7 and 0.9) mol/L was chosen to obtain the optimum conditions for carbon nanopores with high specific surface area. The manufacture of activated carbon is carried out by a one-step pyrolysis technique, namely carbonization and physical activation in one step up to a temperature of 800 °C. Samples LG-0.5, LG-0.7, and LG-0.9 each produced an amorphous structure. Already LG-0.7 has a known combined appearance of hierarchical pores such as sponges and nanofiber pores. This combined pore strongly supports the electrochemical properties of the carbon electrode with 256 F g^{-1}, a specific energy of 35.6 Wh kg^{-1} and a power density of 128.3 W kg^{-1}. These results show the tremendous potential of lemongrass leaf waste as a raw material for the manufacture of porous carbon electrodes for high supercapacitors.

Declaration of Competing Interest

[52]The authors declare that they have no known competing financial interests or personal relationships that could have appeared to influence the work reported in this paper.

Acknowledgement

The work was financially supported by *Kementerian Pendidikan, Kebudayaan, Riset, dan Teknologi*, Repulic of Indonesia through second year Proj[61]of World Class Research (WCR) 2022, contract No: 1627/UN19.5.1.3/PT.01.03/2022.

REFERENCES

[1] Burke A. Ultracapacitors: why, how, and where is the technology. J Power Sources 2000;91:37–50.

[2] Li X, Zhang J, Liu B, Su Z. A critical review on the application and recent developments of post-modified biochar in supercapacitors. J Clean Prod 2021;310:127428. https://doi.org/10.1016/j.jclepro.2021.127428.

[3] González A, Goikolea E, Barrena JA, Mysyk R. Review on supercapacitors: technologies and materials. Renew Sustain Energy Rev 2016;58:1189–206. https://doi.org/10.1016/j.rser.2015.12.249.

[4] Iro ZS, Subramani C, Dash SS. A brief review on electrode materials for supercapacitor. Int J Electrochem Sci 2016;11:10628–43. https://doi.org/10.20964/2016.12.50.

[5] Shukla AK, Banerjee A, Ravikumar MK, Jalajakshi A. Electrochemical capacitors: technical challenges and prognosis for future markets. Electrochim Acta 2012;84:165–73. https://doi.org/10.1016/j.electacta.2012.03.059.

[6] Zhang L, Zhao XS. Carbon-based materials as supercapacitor electrodes. Chem Soc Rev 2009;38:2520–31. https://doi.org/10.1039/b813846j.

[7] Gopalakrishnan A, Badhulika S. Effect of self-doped heteroatoms on the performance of biomass-derived carbon for supercapacitor applications. J Power Sources 2020;480:228830. https://doi.org/10.1016/j.jpowsour.2020.228830.

[8] Lu W, Cao X, Hao L, Zhou Y, Wang Y. Activated carbon derived from pitaya peel for supercapacitor applications with high capacitance performance. Mater Lett 2020;264:127339. https://doi.org/10.1016/j.matlet.2020.127339.

[9] Chiu YH, Lin LY. Effect of activating agents for producing activated carbon using a facile one-step synthesis with waste coffee grounds for symmetric supercapacitors. J Taiwan Inst Chem Eng 2019;101:177–85. https://doi.org/10.1016/j.jtice.2019.04.050.

[10] Luo L, Zhou Y, Yan W, Wu X, Wang S, Zhao W. Two-step synthesis of B and N co-doped porous carbon composites by microwave-assisted hydrothermal and pyrolysis process for supercapacitor application. Electrochim Acta 2020;360. https://doi.org/10.1016/j.electacta.2020.137010.

[11] Cuña A, Tancredi N, Bussi J, Deiana AC, Sardella MF, Violeta B, et al. Grandis as a biocarbons precursor for supercapacitor electrode application. Waste and Biomass Valorization 2014;5:305–13. https://doi.org/10.1007/s12649-013-9257-4.

[12] Taer E, Pratiwi L, Apriwandi, Mustika WS, Taslim R, Agustino. Three-dimensional pore structure of activated carbon monolithic derived from hierarchically bamboo stem for supercapacitor application. Commun Sci Technol 2020;5:22–30. https://doi.org/10.21924/cst.5.1.2020.180.

[13] Misnon II, Zain NKM, Jose R. Conversion of oil palm kernel shell biomass to activated carbon for supercapacitor electrode application. Waste and Biomass Valorization 2019;10:1731–40. https://doi.org/10.1007/s12649-018-0196-y.

[14] Taer E, Hasanah F, Taslim R. Nanofiber-enrich activated carbon coin derived from tofu dregs as electrode materials for supercapacitor. Commun Sci Technol 2021;6:41–8.

[15] Xu H, Zhang Y, Wang L, Chen Y, Gao S. Hierarchical porous biomass-derived carbon framework with ultrahigh surface area for outstanding capacitance supercapacitor. Renew Energy 2021;179:1826–35. https://doi.org/10.1016/j.renene.2021.08.008.

[16] Cao S, Yang J, Li J, Shi K, Li X. Preparation of oxygen-rich hierarchical porous carbon for supercapacitors through the co-carbonization of pitch and biomass. Diam Relat Mater 2019;96:118–25. https://doi.org/10.1016/j.diamond.2019.04.036.

[17] Li X, Wei B. Supercapacitors based on nanostructured carbon. Nano Energy 2013;2:159–73. https://doi.org/10.1016/j.nanoen.2012.09.008.

[18] Azwar E, Wan Mahari WA, Chuah JH, Vo DVN, Ma NL, Lam WH, et al. Transformation of biomass into carbon nanofiber for supercapacitor application-A review. Int J Hydrogen Energy 2018;43:20811–21. https://doi.org/10.1016/j.ijhydene.2018.09.111.

[19] Sodtipinta J, Amornsakchai T, Pakawatpanurut P. Nanoporous carbon derived from agro-waste pineapple leaves for supercapacitor electrode. Adv Nat Sci Nanosci Nanotechnol 2017;8:035017. https://doi.org/10.1088/2043-6254/aa7233.

[20] Yin L, Chen Y, Li D, Zhao X, Hou B, Cao B. 3-Dimensional hierarchical porous activated carbon derived from coconut fibers with high-rate performance for symmetric supercapacitors. Mater Des 2016;111:44–50. https://doi.org/10.1016/j.matdes.2016.08.070.

[21] Taslim R, Hamdy MI, Siska M, Taer E, Yusra DA, Jelita M, et al. Interconnected activated carbon nano fiber derived from mission grass for electrode materials of supercapacitor. Adv Nat Sci Nanosci Nanotechnol 2021;12:35013. https://doi.org/10.1088/2043-6262/ac2953.

[22] Kumari P, Pathak G, Gupta R, Sharma D, Meena A. Cellulose nanofibers from lignocellulosic biomass of lemongrass using enzymatic hydrolysis: characterization and cytotoxicity. DARU J Pharm Sci 2019;27:683–93. https://doi.org/10.1007/s40199-019-00303-1.

[23] Deraman M, Ishak MM, Farma R, Awitdrus, Taer E, Talib IA, et al. Binderless composite electrode monolith from carbon nanotube and biomass carbon activated by H2SO4 and CO2 gas for supercapacitor. AIP Conf Proc 2011;1415:175–9. https://doi.org/10.1063/1.3667250.

[24] Taer E, Apriwandi A, Taslim R, Agutino A, Yusra DA. Conversion Syzygium oleana leaves biomass waste to porous activated carbon nanosheet for boosting supercapacitor performances. J Mater Res Technol 2020;9:13332–40. https://doi.org/10.1016/j.jmrt.2020.09.049.

[25] Chen H, Guo YC, Wang F, Wang G, Qi PR, Guo XH, et al. An activated carbon derived from tobacco waste for use as a supercapacitor electrode material. N Carbon Mater 2017;32:592–9. https://doi.org/10.1016/S1872-5805(17)60140-9.

[26] Taer E, Natalia K, Apriwandi A, Taslim R, Agustino A, Farma R. The synthesis of activated carbon nano fiber electrode made from acacia leaves (Acacia mangium wild) as supercapacitors. Adv Nat Sci Nanosci Nanotechnol 2020;11:25007. https://doi.org/10.1088/2043-6254/ab8b60.

[27] Chang J, Gao Z, Wang X, Wu D, Xu F, Wang X, et al. Activated porous carbon prepared from paulownia flower for high performance supercapacitor electrodes. Electrochim Acta 2015;157:290–8. https://doi.org/10.1016/j.electacta.2014.12.169.

[28] Taer E, Deraman M, Taslim R, Iwantono. Preparation of binderless activated carbon monolith from pre-carbonization rubber wood sawdust by controlling of carbonization and activation condition. AIP Conf Proc 2013;1554:33–7. https://doi.org/10.1063/1.4820277.

[29] Taer E, Apriwandi A, Rama D. Solid coin-like design activated carbon nanospheres derived from shallot peel precursor for boosting supercapacitor performance. J Mater Res Technol 2021;15:1732–41. https://doi.org/10.1016/j.jmrt.2021.09.025.

[30] Pereira RG, Veloso CM, Da Silva NL, De Sousa LF, Bonomo RCF, De Souza AO, et al. Preparation of activated carbons from cocoa shells and siriguela seeds using H3PO4 and ZnCL2 as activating agents for BSA and α-lactalbumin adsorption. Fuel Process Technol 2014;126:476–86. https://doi.org/10.1016/j.fuproc.2014.06.001.

[31] Changmai M, Banerjee P, Nahar K, Purkait MK. A novel adsorbent from carrot, tomato and polyethylene terephthalate waste as a potential adsorbent for Co (II) from aqueous solution: kinetic and equilibrium studies. J Environ Chem Eng 2018;6:246–57. https://doi.org/10.1016/j.jece.2017.12.009.

[32] Pourhosseini SEM, Norouzi O, Naderi HR. Study of micro/macro ordered porous carbon with olive-shaped structure derived from Cladophora glomerata macroalgae as efficient working electrode of supercapacitors. Biomass Bioenergy 2017;107:287–98. https://doi.org/10.1016/j.biombioe.2017.10.025.

[33] Marquez-Montesino F, Torres-Figueredo N, Lemus-Santana A, Trejo F. Activated carbon by potassium carbonate activation from pine sawdust (pinus montezumae lamb.). Chem Eng Technol 2020;43:1716–25. https://doi.org/10.1002/ceat.202000051.

[34] Mensah-Darkwa K, Zequine C, Kahol PK, Gupta RK. Supercapacitor energy storage device using biowastes: a sustainable approach to green energy. Sustain Times 2019;11. https://doi.org/10.3390/su11020414.

[35] Apriwandi A, Taer E, Farma R, Setiadi RN, Amiruddin E. A facile approach of micro-mesopores structure binder-free coin/monolith solid design activated carbon for electrode supercapacitor. J Energy Storage 2021;40:102823. https://doi.org/10.1016/j.est.2021.102823.

[36] Cai Y, Luo Y, Dong H, Zhao X, Xiao Y, Liang Y, et al. Hierarchically porous carbon nanosheets derived from Moringa oleifera stems as electrode material for high-performance electric double-layer capacitors. J Power Sources 2017;353:260–9. https://doi.org/10.1016/j.jpowsour.2017.04.021.

[37] Jiang X, Guo F, Jia X, Zhan Y, Zhou H, Qian L. Synthesis of nitrogen-doped hierarchical porous carbons from peanut shell as a promising electrode material for high-performance supercapacitors. J Energy Storage 2020;30:101451. https://doi.org/10.1016/j.est.2020.101451.

[38] Taer E, Apriwandi, Dalimunthe BKL, Taslim R. A rod-like mesoporous carbon derived from agro-industrial cassava petiole waste for supercapacitor application. J Chem Technol Biotechnol 2021;96. https://doi.org/10.1002/jctb.6579.

[39] Abioye AM, Ani FN. Recent development in the production of activated carbon electrodes from agricultural waste biomass for supercapacitors: a review. Renew Sustain Energy Rev 2015;52:1282–93. https://doi.org/10.1016/j.rser.2015.07.129.

[40] Wan L, Chen D, Liu J, Zhang Y, Chen J, Du C, et al. Facile preparation of porous carbons derived from orange peel via basic copper carbonate activation for supercapacitors. J Alloys Compd 2020;823:153747. https://doi.org/10.1016/j.jallcom.2020.153747.

[41] Gou G, Huang F, Jiang M, Li J, Zhou Z. Hierarchical porous carbon electrode materials for supercapacitor developed from wheat straw cellulosic foam. Renew Energy 2020;149:208–16. https://doi.org/10.1016/j.renene.2019.11.150.

[42] Zhao YP, Xu RX, Cao JP, Zhang XY, Zhu JS, Wei XY. N/O co-doped interlinked porous carbon nanoflakes derived from soybean stalk for high-performance supercapacitors. J Electroanal Chem 2020;871:114288. https://doi.org/10.1016/j.jelechem.2020.114288.

[43] Molina-Sabio M, González MT, Rodriguez-Reinoso F, Sepúlveda-Escribano A. Effect of steam and carbon dioxide activation in the micropore size distribution of activated carbon. Carbon N Y 1996;34:505–9. https://doi.org/10.1016/0008-6223(96)00006-1.

[44] Ding C, Liu T, Yan X, Huang L, Ryu S, Lan J, et al. An ultra-microporous carbon material boosting integrated capacitance for cellulose-based supercapacitors. Nano-Micro Lett 2020;12:63. https://doi.org/10.1007/s40820-020-0393-7.

[45] Tian J, Zhang T, Talifu D, Abulizi A, Ji Y. Porous carbon materials derived from waste cotton stalk with ultra-high surface area for high performance supercapacitors. Mater Res Bull 2021;143:111457. https://doi.org/10.1016/j.materresbull.2021.111457.

[46] Liu F, Wang Z, Zhang H, Jin L, Chu X, Gu B, et al. Nitrogen, oxygen and sulfur co-doped hierarchical porous carbons toward high-performance supercapacitors by direct pyrolysis of kraft lignin. Carbon N Y 2019;149:105–16. https://doi.org/10.1016/j.carbon.2019.04.023.

[47] Xin X, Song N, Jia R, Wang B, Dong H, Ma S, et al. P-codoped porous carbon derived from chitosan with hierarchical N-enriched structure and ultra-high specific surface Area toward high-performance supercapacitors. J Mater Sci Technol 2021;88:45–55. https://doi.org/10.1016/j.jmst.2021.02.014.

[48] Yakaboylu GA, Jiang C, Yumak T, Zondlo JW, Wang J, Sabolsky EM. Engineered hierarchical porous carbons for supercapacitor applications through chemical pretreatment and activation of biomass precursors. Renew Energy 2021;163:276–87. https://doi.org/10.1016/j.renene.2020.08.092.

[49] Hor AA, Hashmi SA. Optimization of hierarchical porous carbon derived from a biomass pollen-cone as high-performance electrodes for supercapacitors. Electrochim Acta 2020;356:136826. https://doi.org/10.1016/j.electacta.2020.136826.

[50] Zhang S, Yin H, Wang J, Zhu S, Xiong Y. Catalytic cracking of biomass tar using Ni nanoparticles embedded carbon nanofiber/porous carbon catalysts. Energy 2021;216:119285. https://doi.org/10.1016/j.energy.2020.119285.

[51] Selvaraj AR, Muthusamy A, In-ho-Cho, Kim HJ, Senthil K, Prabakar K. Ultrahigh surface area biomass derived 3D hierarchical porous carbon nanosheet electrodes for high energy density supercapacitors. Carbon N Y 2021;174:463–74. https://doi.org/10.1016/j.carbon.2020.12.052.

[52] Jiang W, Pan J, Liu X. A novel rod-like porous carbon with ordered hierarchical pore structure prepared from Al-based metal-organic framework without template as greatly enhanced performance for supercapacitor. J Power Sources 2019;409:13–23. https://doi.org/10.1016/j.jpowsour.2018.10.086.

[53] Taer E, Apriwandi A, Agutino A, Taslim R, Mustika WS, Fadli Exa. Surface modification: unique ellipsoidal/strobili-fiber structure of porous carbon monolith for electrode supercapacitor. Nanosci Technol An Int J 2021;12:45–63.

[54] Lämmel C, Schneider M, Weiser M, Michaelis A. Investigations of electrochemical double layer capacitor (EDLC) materials - a comparison of test methods. Mater Werkst 2013;44:641–9. https://doi.org/10.1002/mawe.201300122.

[55] Zhang Y, Yu S, Lou G, Shen Y, Chen H, Shen Z, et al. Review of macroporous materials as electrochemical supercapacitor electrodes. J Mater Sci 2017;52:11201–28. https://doi.org/10.1007/s10853-017-0955-3.

[56] Yao Y, Chen X, Yu N, Wei F, Feng H. Preparation and supercapacitive performance of lead dioxide electrodes with three-dimensional porous structure. Russ J Electrochem 2018;54:585–91. https://doi.org/10.1134/S1023193518070078.

[57] Şirazi M, Aslan S. Comprehensive characterization of high surface area activated carbon prepared from olive pomace by KOH activation. Chem Eng Commun 2021;0:1–15. https://doi.org/10.1080/00986445.2020.1864628.

[58] Tsai C, Tai H, Su C, Chiang L, Li Y. Activated microporous carbon nanospheres for use in supercapacitors. Appl Nano Mater 2020;3(10):10380–8. https://doi.org/10.1021/acsanm.0c02291.

Interconnected micro-mesoporous carbon nanofiber derived from lemongrass for high symmetric supercapacitor performance

ORIGINALITY REPORT

12%	7%	4%	5%
SIMILARITY INDEX	INTERNET SOURCES	PUBLICATIONS	STUDENT PAPERS

PRIMARY SOURCES

1	Submitted to Nelson Mandela Metropolitan University Student Paper	<1%
2	thesis.univ-biskra.dz Internet Source	<1%
3	Submitted to Universiti Putra Malaysia Student Paper	<1%
4	acsir.res.in Internet Source	<1%
5	Submitted to KYUNG HEE UNIVERSITY Student Paper	<1%
6	Sang-Hoon Park, Hyun-Kyung Kim, Seung-Beom Yoon, Chang-Wook Lee, Dongjoon Ahn, Sang-Ick Lee, Kwang Chul Roh, Kwang-Bum Kim. "Spray-Assisted Deep-Frying Process for the In Situ Spherical Assembly of Graphene for Energy-Storage Devices", Chemistry of Materials, 2015 Publication	<1%

7	biblio.cinvestav.mx Internet Source	<1 %
8	www.hilarispublisher.com Internet Source	<1 %
9	ddd.uab.cat Internet Source	<1 %
10	www.authormapper.com Internet Source	<1 %
11	Submitted to Coventry University Student Paper	<1 %
12	file.scirp.org Internet Source	<1 %
13	ls00012.mah.se Internet Source	<1 %
14	research.abo.fi Internet Source	<1 %
15	Taer, E., M. Deraman, R. Taslim, and Iwantono. "Preparation of binderless activated carbon monolith from pre-carbonization rubber wood sawdust by controlling of carbonization and activation condition", AIP Conference Proceedings, 2013. Publication	<1 %
16	Submitted to University of Wollongong Student Paper	<1 %

17	Submitted to Visvesvaraya National Institute of Technology Student Paper	<1%
18	Submitted to University of Northumbria at Newcastle Student Paper	<1%
19	manu60.magtech.com.cn Internet Source	<1%
20	Reza Lotfi Mayan Sofla, Mostafa Rezaei, Amin Babaie, Mortaza Nasiri. "Preparation of electroactive shape memory polyurethane/graphene nanocomposites and investigation of relationship between rheology, morphology and electrical properties", Composites Part B: Engineering, 2019 Publication	<1%
21	nano.qust.edu.cn Internet Source	<1%
22	Gomibuchi, E.. "Electrode properties of a double layer capacitor of nano-structured graphite produced by ball milling under a hydrogen atmosphere", Carbon, 200604 Publication	<1%
23	Mantravadi, Ramya, Parameswara Rao Chinnam, Dmitriy A Dikin, and Stephanie L. Wunder. "High Conductivity, High Strength	<1%

	Solid Electrolytes Formed by in situ Encapsulation of Ionic Liquids in Nanofibrillar Methyl Cellulose Networks", ACS Applied Materials & Interfaces Publication	
24	Submitted to University of Adelaide Student Paper	<1 %
25	orbit.dtu.dk Internet Source	<1 %
26	research.usq.edu.au Internet Source	<1 %
27	www.journals.elsevier.com Internet Source	<1 %
28	Submitted to King Abdullah University of Science and Technology (KAUST) Student Paper	<1 %
29	sophiapublisher.com Internet Source	<1 %
30	www.aminer.org Internet Source	<1 %
31	www.sciencerepository.org Internet Source	<1 %
32	Afsaneh Noormandi, Iman Karimzadeh, Mahtabalsadat Mirjalili, Hossein Khalili. "Clinical and economic impacts of clinical pharmacists' interventions in Iran: a	<1 %

	systematic review", DARU Journal of Pharmaceutical Sciences, 2019 Publication	
33	Submitted to University of Strathclyde Student Paper	<1 %
34	buscador.una.edu.ni Internet Source	<1 %
35	www.kiche.or.kr Internet Source	<1 %
36	ejournal2.undip.ac.id Internet Source	<1 %
37	isiarticles.com Internet Source	<1 %
38	www.begellhouse.com Internet Source	<1 %
39	Submitted to Skolkovo Institute of Science and Technology (Skoltech) Student Paper	<1 %
40	Submitted to University of Kent at Canterbury Student Paper	<1 %
41	Submitted to University of Petroleum and Energy Studies Student Paper	<1 %
42	foodeng.wisc.edu Internet Source	<1 %

43	Submitted to CSU, San Jose State University Student Paper	<1 %
44	conference.binus.ac.id Internet Source	<1 %
45	www.nmlett.org Internet Source	<1 %
46	Shukla, Ashok, Anjan Banerjee, and Musuwathi Ravikumar. "Lead–Carbon Hybrid Ultracapacitors and Their Applications", Electrochemically Enabled Sustainability, 2014. Publication	<1 %
47	Submitted to Indian Institute of Technology Student Paper	<1 %
48	K. S. W. Sing. "Reporting physisorption data for gas/solid systems with special reference to the determination of surface area and porosity (Provisional)", Pure and Applied Chemistry, 1982 Publication	<1 %
49	Qian He, Ying Wang, Xiong Xiong Liu, Daniel John Blackwood, Jun Song Chen. " One-pot synthesis of self-supported hierarchical urchin-like Ni S with ultrahigh areal pseudocapacitance ", Journal of Materials Chemistry A, 2018 Publication	<1 %

50	cemse.kaust.edu.sa Internet Source	<1 %
51	iknow-imeri.fk.ui.ac.id:8080 Internet Source	<1 %
52	livrepository.liverpool.ac.uk Internet Source	<1 %
53	research.manchester.ac.uk Internet Source	<1 %
54	research.utwente.nl Internet Source	<1 %
55	www.differ.nl Internet Source	<1 %
56	Neeraj Sharma, Alka Tiwari. " Nanomagnetite-loaded poly (acrylamide-co-itaconic acid) hydrogel as adsorbent for effective removal of Mn from contaminated water ", Desalination and Water Treatment, 2015 Publication	<1 %
57	Subramanian, V.. "Synthesis and electrochemical characterizations of amorphous manganese oxide and single walled carbon nanotube composites as supercapacitor electrode materials", Electrochemistry Communications, 200605 Publication	<1 %
	Submitted to University of Leicester	

58	Student Paper	<1%
59	Valery Konopsky, Valery Prokhorov, Dmitry Lypenko, Artem Dmitriev, Elena Alieva, Giovanni Dietler, Sergey Sekatskii. "Electrical Excitation of Long-Range Surface Plasmons in PC/OLED Structure with Two Metal Nanolayers", Nano-Micro Letters, 2020 Publication	<1%
60	Wang, S.. "Physical and chemical regeneration of zeolitic adsorbents for dye removal in wastewater treatment", Chemosphere, 200609 Publication	<1%
61	Zetra Hainul Putra, Ramiati, Zufriady, Riyan Hidayat, Jismulatif, Neni Hermita, Urip Sulistiyo. "Development of computational thinking tasks based on Riau Malay culture: a study of fifth-grade public school students in Pekanbaru, Indonesia", Education 3-13, 2022 Publication	<1%
62	akjournals.com Internet Source	<1%
63	da Cruz, José Alberto, Jefferson José Vilela, Berenice Mendonça Gonzalez, and Dagoberto Brandão Santos. "Effect of Retained Austenite on Impact Toughness of the Multi-Phase	<1%

Bainitic-Martensitic Steel", Advanced Materials Research, 2014.
Publication

64	etdci.org Internet Source	<1%
65	ktisis.cut.ac.cy Internet Source	<1%
66	pure.au.dk Internet Source	<1%
67	research-information.bris.ac.uk Internet Source	<1%
68	scholarworks.unist.ac.kr Internet Source	<1%
69	www.science.org Internet Source	<1%
70	Yanwu Zhu, Shanthi Murali, Weiwei Cai, Xuesong Li, Ji Won Suk, Jeffrey R. Potts, Rodney S. Ruoff. "Graphene and Graphene Oxide: Synthesis, Properties, and Applications", Advanced Materials, 2010 Publication	<1%

Exclude quotes	Off	Exclude matches	Off
Exclude bibliography	Off		